Book of Tutorials and Abstracts

European Microbeam Analysis Society

EMAS 2019

16th

EUROPEAN WORKSHOP

on

MODERN DEVELOPMENTS AND APPLICATIONS IN MICROBEAM ANALYSIS

19 to 23 May 2019
at the
NTNU, Realfagbygget
Trondheim, Norway

Organised in collaboration with:
Norwegian University of Science and Technology
(NTNU)

RECENT PROGRESSES IN SOFT X-RAY EMISSION SPECTROSCOPY

Masami Terauchi[1,*], T. Hatano[1], M. Koike[2], A.S. Pirozhkov[2], H. Sasai[3], T. Nagano[3], M. Takakura[4] and T. Murano[4]

1 Tohoku University, IMRAM
2-1-1 Katahira, 980-8577 Sendai, Japan
2 National Institute for Quantum and Radiological Science, QuBS Directorate,
619-0215 Kizugawa, Japan
3 SHIMADZU Corp., Device Department,
604-8511 Kyoto, Japan
4 JEOL Ltd., SA Business Unit
196-8558 Akishima, Japan
e-mail: terauchi@m.tohoku.ac.jp

Masami Terauchi is a professor in the Institute of Multidisciplinary Research for Advanced Materials at Tohoku University. He started his research carrier with convergent-beam electron diffraction (CBED) studies of crystal structure change at phase transitions, phason strains in quasicrystals and incommensurately modulated structures. Then, moved to development of a high energy-resolution electron energy-loss spectroscopy (EELS) electron microscope. Dielectric properties and density of states of carbon and fullerene materials, quasi-crystalline alloys, boron-related materials were investigated. This development and applications triggered commercialisation projects of monochromator TEM. From around 2000, he started to develop a soft X-ray emission spectroscopy (SXES) instrument for TEM. It aimed to obtain information of bonding electrons, which cannot by EELS. Based on the developed spectrometer, a commercial SXES system was commercialized for EPMA and SEM. The improvements of the spectrometer, its applications and making a data booklet are now on the way.

1. INTRODUCTION

Observing fine structures of materials and atomic arrangements, and examining compositional elements and those chemical states are the key issues asked for recent electron microscopy. Especially, chemical state of element related to material's function is a core of interest for material's scientists and companies. Recent dedicated transmission electron microscope (TEM) is a powerful and widely used tool for analysing the crystalline order and orientation by electron diffraction pattern, lattice defects by Bragg contrast imaging, atomic arrangements by phase-contrast and/or high-angle dark-field contrast imagines, the composition by X-ray emission spectroscopy (energy-dispersive spectroscopy, EDS), and chemical state analysis by electron energy-loss spectroscopy (EELS) of nm-scale specimen areas. Those capabilities of TEM can only be applied for thin specimens. On the other hand, a chemical state analysis method for bulk specimens based on electron microscopy has not been well established in energy resolution compare with those of EELS experiments of 0.1 - ~1 eV. In the last twenty years, soft X-ray emission spectroscopy (SXES) instruments for electron microscopes have been developed based on TEM and examined its possibilities [1]. After that, the instrument was applied for scanning electron microscope (SEM) and also commercialised as an attachment for electron probe microanalyser (EPMA) and/or SEM [2, 3].

The optics and structure of SXES spectrometer for electron microscopes, experimental results showing the possibility of chemical state analysis and its imaging of bulk specimens and recent developments for the next generation are shown below.

2. X-RAY EMISSION DUE TO ELECTRONIC TRANSITION AND ITS INFORMATION

High energy electron-beam irradiation for a specimen creates a core-hole by exciting a core-electron and successively happen an X-ray emission as a relaxation process owing to a transition of an electron to the core-hole state. Figure 1 shows a schematic drawing of electronic transitions among conduction bands (CB), valence bands (VB), and inner-shell levels. The excitation processes, upward arrows, are used in EELS to examine a chemical state of a material. The relaxation processes, downward arrows, are used in X-ray emission spectroscopy (XES) for elemental analysis and/or phase identifications as wavelength-dispersive X-ray spectroscopy (WDS) and energy-dispersive X-ray spectroscopy (EDS).

Valence electron excitation EELS spectra (process **a**) include information of band-gap and interband transition energies and refractive indices. This experimental results can be compared with optical experiments by using Kramers-Kronigh analysis. Inner-shell electron excitation EELS spectra (process **b**) give us information of the density of states (DOS) of CB (anti-bonding states). This inner-shell excitation spectroscopy corresponds to X-ray absorption experiments. Together with the DOS of CB, the DOS of VB (bonding states) is necessary to understand the whole electronic structure of a material. This is important because the origin of stabilizing a

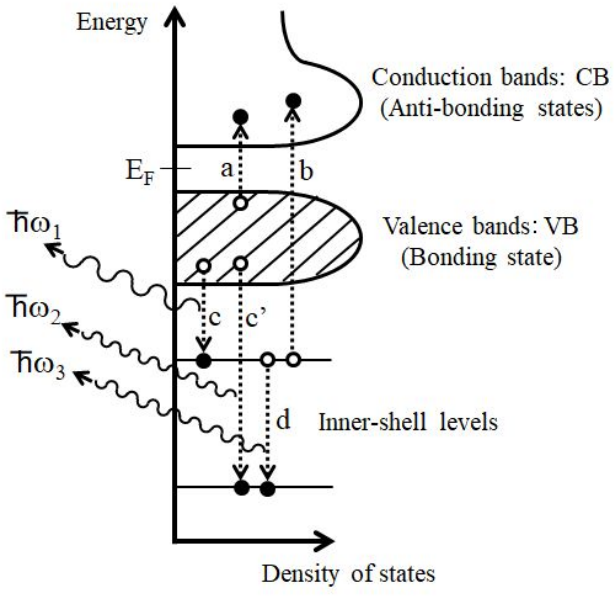

Figure 1. Schematic diagram of electronic structure and electronic transitions related to EELS (a and b), and XES (c, c' and d).

material is the energy states of bonding electrons. This information is included in the joint DOS of CB and VB (the imaginary part of ε, ε_2). However, it is not possible to deduce the information from ε_2, because of a lack of information of energy dispersion of bonding states.

Electronic transitions, downward arrows in Fig. 1, from VB to inner-shell core-hole states (processes **c**, **c'**) and from a shallow core-level to a deeper-lying core-level (process **d**) accompanied by X-ray emission. Thus, X-ray emissions caused by the process **c** and **c'** include information of energy distribution of bonding electrons, DOS of VB. An energy resolution better than 1 eV is necessary for obtaining fine structures of the DOS of VB, because the energy spread of VB is usually from 5 to 10 eV. Since the transitions can happen under a dipole-selection condition ($\Delta l = \pm 1$), the intensity profile of an emission spectrum reflects a partial DOS of VB with a specific symmetry. Furthermore, X-ray emission spectra of different atoms of a compound show us the component of different atoms of the valence DOS. Those emission energies range in the soft X-ray energy region from 15 to 6,000 eV [4]. Since there are many atomic resonances in this energy region, soft X-ray emission spectroscopy (SXES) provides not only the compositional information but also chemical states of elements, a sensitive tool for elemental and chemical identification, which can make many application opportunities. On the other hand, X-ray emissions caused by the electronic transition **d** between inner-shell levels does not contain the information of bonding electrons.

SXES is a one candidate for valence electron spectroscopy based on electron microscopy. This method does not need an ultra-high-vacuum condition, because the absorption length of soft X-rays is larger than surface thickness of a few tens nm [5]. Then, it can be combined with conventional electron microscopes of SEM and TEM. One drawback of this method is the low

emission efficiency. For example, the yield of X-ray emission of a carbon 1s core-hole state is 2.8 x 10^{-3} [6]. Then, a longer acquisition time is necessary compared to those of EELS experiments. This is why SXES spectrometer was commercialised for EPMA and SEM.

Another point should be taken into account for obtaining DOS of VB is a natural width, lifetime broadening, of an inner-shell level concerned [7]. This natural broadening is directly related to the fluorescent yield of each transition. The initial state for X-ray emission, a highly excited state having an inner-shell core-hole, can decay to the lower excited states or the ground state by X-ray emission, Auger electron emission, and a creation of another core-hole state via Coster-Kronig process. A high yield for X-ray emission, a short lifetime, causes a larger natural width. For example, the emission yield and the natural width of Cu-L3 level are 6 x 10^{-3} and 0.56 eV, respectively. Then, an instrumental energy resolution of 0.8 eV is necessary for realising 1 eV resolution for Cu-Lα emission (3d→L3; 930 eV). Other origins for level broadenings can be a multiple splitting of inner-shell level, and a multiple ionisation of atom.

3. OPTICS OF SXES SPECTROMETERS

SXES instrument developed for conventional EPMA/SEM does not have a moving mechanism as for Rowland mounting optics of a traditional EPMA. The SXES spectrometer adopts the flat-field grazing-incidence optics by using varied-line-spacing (VLS) gratings [8, 9]. Figure 2 shows a schematic figure of the optics of a spectrometer. This optics is rather compact, about 50 cm from the specimen to the detector. This compact size means smaller energy dispersion on the spectrum plane. Then, a smaller pixel sized detector is crucial for this optics to obtain a reasonable energy resolution. As the VLS grating forms a spectrum in a certain energy range on a flat plane, a parallel detection by using a CCD detector is realised. The energy resolution was evaluated to be about 0.2 eV for Al L-emission with the commercial system. The grating works for a fixed grazing incidence angle, which ranges from 1.5 to 4 degrees depending on the design of the acceptance energy range of the grating. This small grazing incidence angle improves a reflection efficiency of the grating, but causes a small solid-angle for detection. For improving detection efficiency, X-ray correction mirrors have been designed and placed between a specimen positon and the VLS grating. The mirrors increase the detection solid angle of this SXES instruments by a factor of 2 - 3.

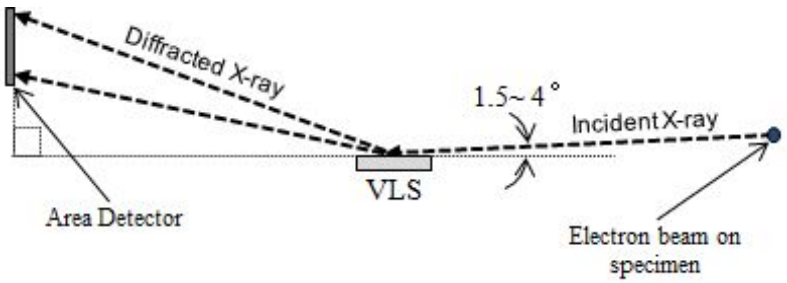

Figure 2. Schematic optics of VLS grating used.

The original optics was designed to cover from 50 to 3,800 eV by using four VLS gratings, whose optics is also adopted the flat-field grazing-incidence [10, 11]. Two spectrometers of this optics were installed to a TEM [10, 11] and a SEM [2, 12]. As a present commercial instrument can accommodate only two VLS gratings, the detection energy range is limited compared with the original one. Figure 3 shows a photo of the spectrometer with four VLS gratings attached to a conventional SEM. A fine-pitch micro-channel plate (MCP) optically coupled with a CMOS camera is used as a detector. This detection system performs an energy resolution of 0.08 eV for Al L-emission in photon-counting operation mode. This means that the energy resolution of commercial spectrometer is limited by a pixel size of a detector.

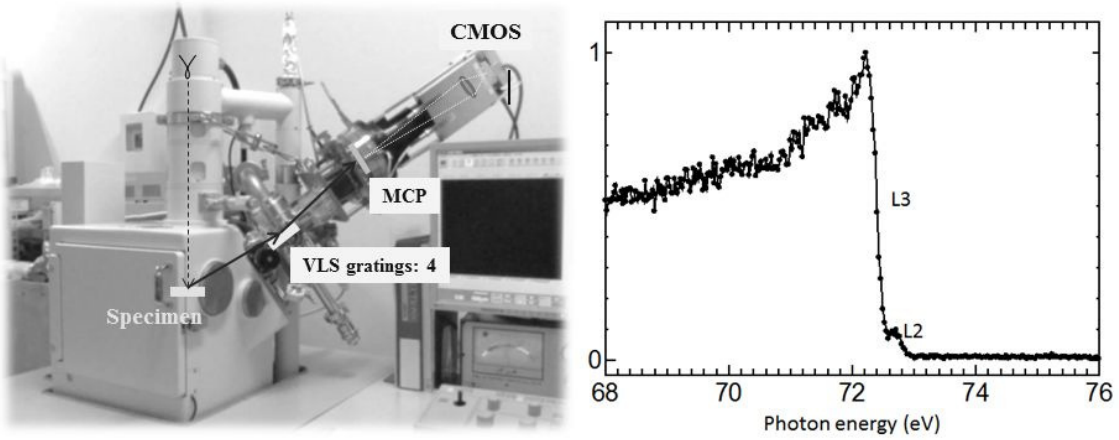

Figure 3. Photo of a SEM-SXES instrument for 50 - 3,800 eV and a spectrum of Al L-emission with an energy resolution of 0.08 eV.

4. SXES SPECTRA REFLECTING BONDING STATES AND ITS IMAGING

Figure 4 shows B K-emission spectra of CaB_6 and CeB_6 . Those are composed of a network of B_6 octagonal clusters accommodating a metal atom at the body-centre positon of the unit cell, as shown in an inset figure. An B K-emission spectrum of β-rhombohedral boron (β-r-B), which is classified to a B_{12}-cluster material, is also shown for comparison. Peak intensity at around 185 eV in each spectrum is due to intra-cluster bonding state. The tail intensity in the lower energy side is due to inter-cluster bonding states. In case of CaB_6, Ca atom can transfer two valence electrons to the B_6 cluster network. Then, VB of B_6-cluster network is fully occupied and becomes a semiconductor. On the other hand, Ce atom can transfer 3 or 4 electrons to B_6-clusteer network. Thus, excess electrons go into CB and becomes a metal B_6-material. This can be seen in the intensity profile of CeB_6. In the higher energy side of the main peak, there is an additional intensity compared with that of CaB_6. This additional intensity due to electrons occupying CB. A small onset in the right hand side end of the additional intensity should correspond to Fermi energy position of the material.

Furthermore, it can be notice that main peak position of CeB_6 is a little shifted in lower energy side compared with that of CaB_6. As B K-emission is due to transitions form VB to B1s core-level, this shift can be assign as a chemical shift of B1s core-level due to a larger amount of charge transfer of Ce atom than Ca atom.

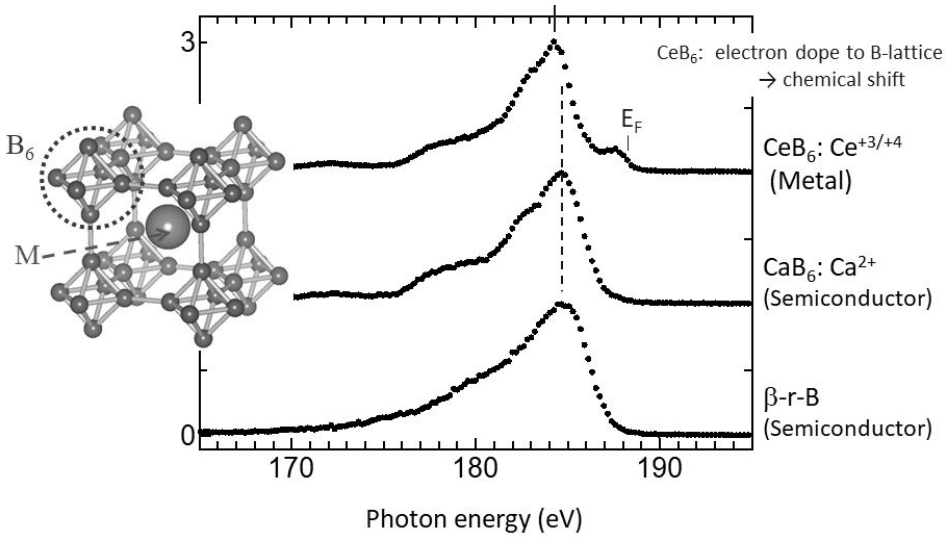

Figure 4. B K-emission spectra of CaB_6, CeB_6 and β-rhombohedral boron (β-r-B). The spectrum of CeB_6 shows an additional intensity with Fermi edge in right hand side and a peak shift, chemical shift, due to a larger amount of charge transfer of Ce atom than that of Ca.

CaB_6 is a n-type semiconductor. For realizing a thermo-electric device using B_6-cluster network materials [13], p-type semiconductor is necessary. As Na atom has only one valence electron, Na substitution to Ca site of CaB_6 (Na-doped CaB_6) realises a hole doping to B_6-cluster network, causing a p-type semiconductor as a bulk [14]. From an EDS evaluation, Na content of the material was a few percent. However, the material may be not a uniform from a production process point of view. Then, a piece of Na-doped CaB_6 bulk specimen was evaluated by using a commercial EPMA-SXES instrument. Figure 5 shows spectral intensity maps of (a) Ca-Lℓ, η intensity (150 - 154 eV), (b) B-K intensity (170 - 188 eV), and (c) the top part of the B-K intensity (187 - 188 eV). Ca-Lℓ, η emission map shows a low intensity in the central area. It means a low Ca content for the area. B-K emission map shows a little intensity change for the corresponding area. An intensity anomaly in the upper left of the image is due to a surface contamination. The composition and chemical bonding state of the central area may be different form the surrounding area. Spectral map of the top part of the B-K emission intensity in Fig. 5c shows an apparent intensity increase for the central area. For investigate the origin of this intensity increase, B-K emissions spectra of the points of A and B indicated in Fig. 5c are shown in the left bottom. The spectra show a little difference in those intensity distributions, suggesting some difference of bonding state of B_6-cluster network due to a difference in composition. When

considering peak (arrow) position, the spectrum A positions in higher energy side by about 0.7 eV compared to that of spectrum B. This shift of the whole spectrum should be due to a chemical shift originated from a larger binding energy of B1s level of the area. The shift can be explained by a decrease of valence charge of B atoms of point A. It can be made by the expected Na-substitution of a smaller charge transfer and/or impurity of oxygen which adopt two electrons from B_6-network. Unfortunately, Na K-emission intensity is the out of the acceptable energy range of the JS200N grating used (the latest commercial system can detect the Na K-emission signal). Impurity oxygen atom cannot be eliminated because a small intensity at 175 eV in the spectrum A can be assign to the 3rd order intensity of O-K emission. In anyway, a high energy resolution SXES mapping can give us not only an elemental map but also a chemical bonding state map reflecting a valence charge distribution. This chemical state mapping combined with elemental map by EPMA/SEM-SXES system gives an important information for phase identification of bulk specimen.

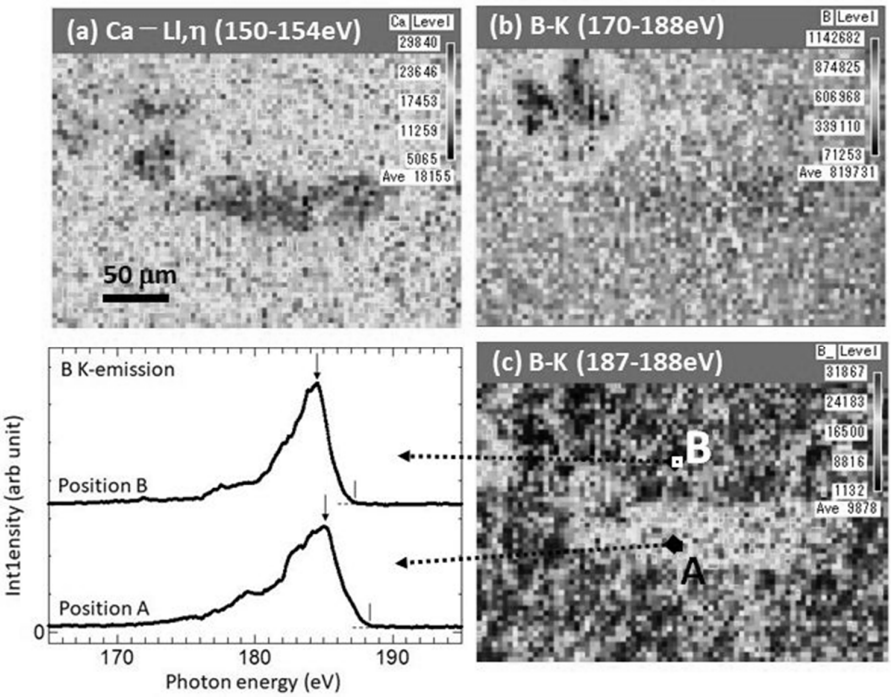

Figure 5. a) Ca-Lℓ, η intensity (150 - 154 eV), b) B-K intensity (170 - 188 eV), c) the top part of the B-K intensity (187 - 188 eV), and B K-emission spectra of the areas A and B in (c).

5. INFORMATION OF L-EMISSION OF TRANSITION METAL ELEMENTS

Bonding state and valence charge of 3d transition metal (3d-TM) elements is a key for evaluating positive electrode materials of Li-ion battery, because a change of valence charge of 3d-TM elements is an origin of charge and discharge performance of the battery. Information of valence

electrons of 3d-TM elements is included in L-emissions of the elements. There are four types of L-emissions of Lα, Lβ, Lℓ and Lη as shown in Fig. 6 [15]. Those are classified into two having close emission energies of Lα,β and Lℓ,η. As Lα,β emission is due to $3d_{5/2,3/2} \rightarrow 2p_{3/2,1/2}$ ($L_{2,3}$) electronic transition, its energy distribution contains an information of DOS of VB (bonding states). On the other hand, Lℓ,η emission energy due to transitions from a shallow inner-shell of $M_1(3s_{1/2})$ to a deeper inner-shell of $L_{2,3}$ reflects the dielectric environment of transition metal elements [16], which is different information from that of Lα,β emissions.

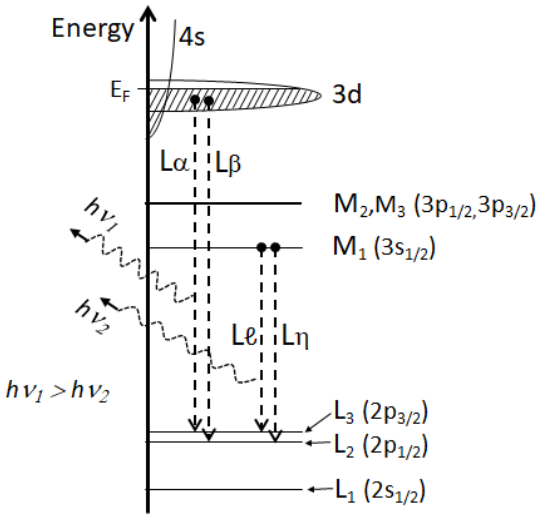

Figure 1. Schematic energy diagram of 3d transition metal elements and electronic transitions of four L-emissions [15].

Figure 7 shows L-emission spectra of simple metal materials of Sc (Z = 21, $3d^14s^2$), Ti (Z = 22, $3d^24s^2$), V (Z = 23, $3d^34s^2$), Cr (Z = 24, $3d^54s^1$), Mn (Z = 25, $3d^54s^2$), Fe (Z = 26, $3d^64s^2$), Co (Z = 27, $3d^74s^2$), Ni (Z = 28, $3d^84s^2$), Cu (Z = 29, $3d^{10}4s^1$) and Zn (Z = 30, $3d^{10}4s^2$) by using the SEM-SXES instrument shown in Fig. 3 [15]. Each spectrum intensity is normalised by its maximum intensity in each spectrum. The grating of JS2000, which covers from 300 eV to 2,200 eV, was used. For aiming a quantitative evaluation, spectral intensities were detected by a MCP detector in photon counting mode, which means that the integrated intensity of an emission peak corresponds to a number of emitted X-ray photons or related electronic transitions in a specimen examined. It is clearly seen that L-emission energy increases with an increase of Z, which is caused by an increase of the binding energy of $L_{2,3}$ level according to Z. Furthermore, the intensity ratio of Lα,β/Lℓ,η increase according to an increase of N_{3d}. This tendency of Lα,β/Lℓ,η is reasonable because the electron number contributed for Lℓ,η emission is constant of two 3s electrons whereas that for Lα,β emission, number of 3d electrons ($N3_d$), increases with Z. Thus, the intensity ratio of Lα,β/Lℓ,η can be an indicator for evaluating N_{3d}. Integrated intensities of Lα,β and Lℓ,η were evaluated from Fig. 7. The intensity ratio of Lα,β/Lℓ,η increases according to N_{3d}, but not linear. As two transition of $3d_{5/2,3/2} \rightarrow L_{2,3}$ and $M_1(3s_{1/2}) \rightarrow L_{2,3}$ are competing in L-emission process, the transition probability of $3d_{5/2,3/2} \rightarrow L_{2,3}$ should change according to a change of N_{3d}. Then, intensity of Lα,β compared

with the whole L-emission intensity of Lα,β + Lℓ,η, which should reflect not only the number of 3d electrons but also a change of transition probability due to a change of N_{3d}, was evaluated. Figure 8 shows the variation of Lα,β(Lα,β + Lℓ,η) according to N_{3d}, which is almost linear from Sc to Ni, except Cr. The deviation of Cr value from an expected gradual increase may reflect a characteristic electron configuration in 3d orbitals. The linear tendency of Lα,β(Lα,β + Lℓ,η) was fitted by a linear equation and applied to some oxides. In case of 3d metal oxides, the evaluation by using the equation was over estimate the number of 3d electrons. It can be assigned to be due to a charge transfer from ligand oxygen atoms to a 3d transition metal element owing to a core-hole effect in the intermediate state as reported by Grebennikov *et al.* [17].

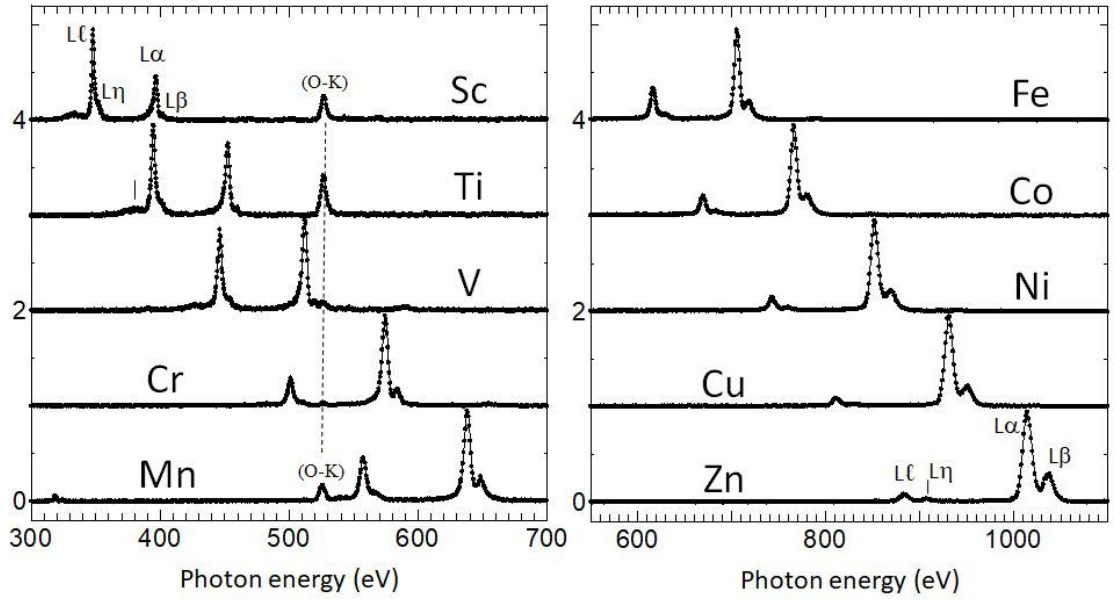

Figure 7. L-emission spectra of simple metal materials of Sc, Ti, V, Cr, Mn, Fe, Co, Ni, Cu and Zn. Each spectrum intensity is normalised by its maximum intensity in each spectrum [15].

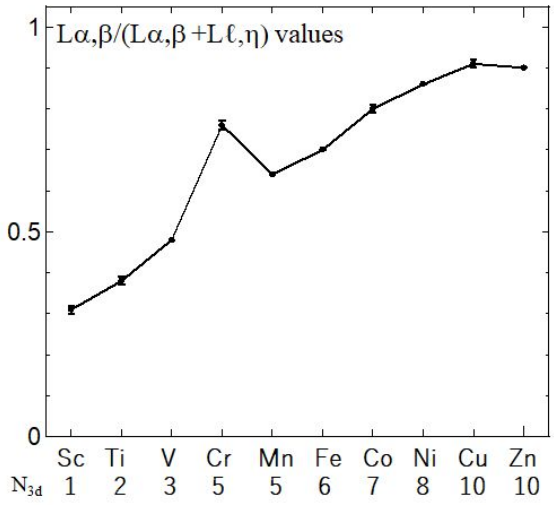

Figure 8. Experimentally obtained Lα,β(Lα,β + Lℓ,η) values for 3d transition metal materials.

6. IMPROVEMENT OF DETECTION EFFICIENCY

As mentioned in section 3, the grazing incidence optics intrinsically has a small solid angle for X-ray detection, even though the grazing incidence improves the reflectance of the grating and this optics can realise a parallel detection in a certain energy range by using a flat detector. For further improvement of detection efficiency, a new optics combined with an enhancement of diffraction efficiency of VLS grating by a coating was designed, manufactured and tested [18]. As a one target, boron was selected because boron is contained at ppm level in steel compounds and works as a key element to improve structural and mechanical properties.

A conventional JS200N, nickel (Ni) coated VLS grating, used in a commercial SXES instrument has a grazing incidence angle of 3°. In the new optics, this angle was changed to 5.8° keeping the positions of a specimen and a detector unchanged. This improves the solid angle by about two times. Furthermore, grating surface of Ni is over coated by La and additionally carbon (JS200NLC). The carbon layer was added to prevent from oxidation of the La layer. This coating is expected to perform a two times larger diffraction efficiency for B K-emission from the theoretical evaluation. Totally, about four times improvement for B-K intensity was expected compared with that of JS200N. A manufactured new grating was tested at synchrotron facility and performed about 5 times improvement at the best condition. The same grating was tested also by using SEM-SXES instrument (Fig. 3), which was modified to realize a new optics. Figure 9 shows a result of B K-emission measurement by using the SEM-SXES instrument. As show in the figure improvement of detected spectral intensity was 3.4 times. This value smaller than five evaluated at synchrotron is due to the unjustified X-ray correction mirrors placed between the specimen and the VLS grating. When compared with the new grating of Ni surface, enhancement was 2.5 times. This means that about five times enhancement is expected for this NI/La/C grating when the X-ray collecting mirrors works as that for JS200N. As La is an active material, a stable compound of LaF_3 was coated on a new grating and tested. For this grating, the diffraction efficiency for B-K was 2.1 times compared with that of Ni surface grating. Then, totally about 4 times improvement is expected.

7. HIGH ENERGY-DISPERSION SPECTROMETER FOR EPMA

Improvement of energy resolution is also important. As mentioned in section 3, the energy resolution of the commercial SXES spectrometer is limited by a pixel size of the CCD detector. There are two candidates to improve the energy resolution. One is to use a fine pitched new detector. Another one is to construct a spectrometer with a larger energy-dispersion. A larger dispersion spectrometer was already designed and constructed for TEM [19]. Figure 10 shows the optics of the spectrometer. The distance from VLS grating to a detector is about two times larger than that of a usual spectrometer. This means that the two time larger energy-dispersion is expected for this optics. However, a larger spectrometer has a small solid-angle for X-ray detection and was not easy to obtain a good signal to noise ratio with TEM. Thus, applying this

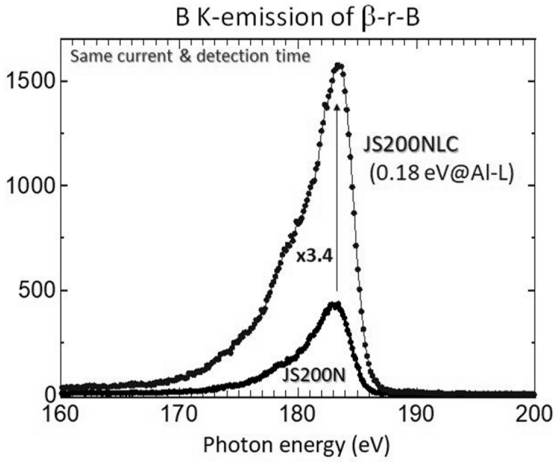

Figure 9. Intensity enhancement of a new grating of JS200NCL compared with a conventional grating of JS200N obtained by SEM-SXES instrument (Fig. 3).

larger spectrometer to EPMA is reasonable to improve in energy resolution with a better signal to noise ratio. Figure 11 shows a photo of a newly (just) constructed SXES spectrometer with the optics of Fig. 10 attached to EPMA, which already has a commercial spectrometer. Two VLS grating are accommodated and covering from B-K to Mg-K, which covering a whole energy range of L-emissions of 3d-TM elements. The detector is a normal MCP optically coupled with a CCD camera.

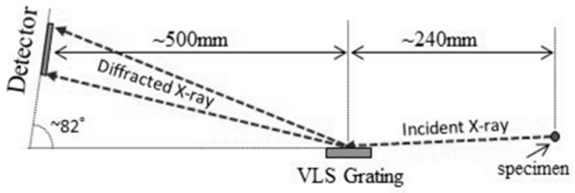

Figure 10. Optics of a larger-dispersion VLS grating.

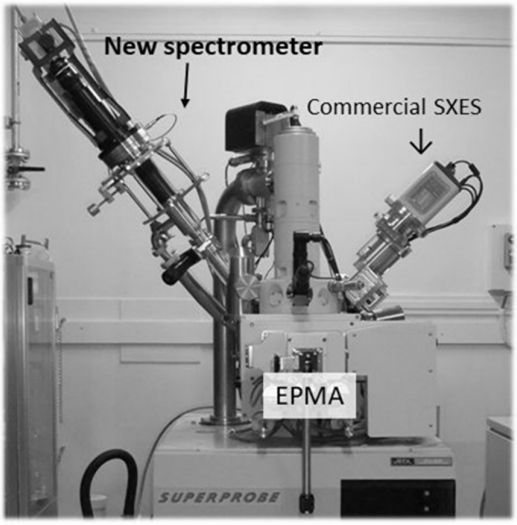

Figure 11. Photo of a newly constructed large-dispersion SXES spectrometer attached to EPMA.

When applying a fine pitch MCP detector already used in SEM-SXES of Fig. 3, the energy resolution becomes more than three times better than that of a commercial spectrometer. This performance will be useful for investigating a chemical state of 3d transition metal elements and its imaging.

8. SUMMARY

After the developments of SXES spectrometers for TEM, SXES spectrometer has commercialised as an attachment for EPMA and SEM. This system has a much better energy resolution owing to a high quality VLS gratings combined with a CCD detector and a high detection efficiency owing to a parallel detection. It realised not only a compositional analysis but also a chemical state analysis and its imaging. For aiming a much higher detection efficiency, a new optics and a new coated grating, which can tune the target energy range, was tested and found a five times improvement is possible for B K-emission. A higher energy resolution targeting a chemical state of 3d-TM elements has just constructed.

9. ACKNOWLEDGEMENTS

Results of metal-B6 materials are collaborated ones with Prof M. Takeda of Nagaoka University of Technology, Nagaoka, Japan. This work was partly supported by the Research Programme of "Dynamic Alliance for Open Innovation Bridging Human, Environment and Materials" in "Network Joint Research Centre for Materials and Devices".

10. REFERENCES

[1] Terauchi M 2014 Valence electron spectroscopy for transmission electron microscopy. in: Characterization tools for nanoscience and nanotechnology. (Kumar C S S R; Ed.) (Springer-Verlag Berlin Heidelberg) 287-331

[2] Terauchi M, Koshiya S, Satoh F, Takahashi F, Handa N, Murano T, Koike M, Imazono T, Koeda M, Nagano T, Sasai H, Oue Y, Yonezawa Z and Kuramoto S 2014 Chemical state information of bulk specimens obtained by SEM based soft-X-ray emission spectroscopy. *Microsc. Microanal.* **20** 692-697

[3] Takahashi H, Handa N, Murano T, Terauchi M, Koike M, Kawachi T, Imazono T, Hasegawa N, Koeda M, NaganoT, Sasai H, Oue Y, Yonezawa Z and Kuramoto S 2014 Exciting possibilities of soft X-ray emission spectroscopy as chemical state analysis in EPMA and FESEM. *Microsc. Microanal.* **20** (Suppl. 3) 684-685.

[4] Fabian D J, Watson L M and Marshall C A W 1972 Soft X-ray spectroscopy and the electronic structure of solids. *Rep. Prog. Phys.* **34** 601-696

[5] Attwood D 2000 *Soft X-rays and extreme ultraviolet radiation*. (Cambridge, UK: Cambridge University Press)

[6] Krause M O 1979 Atomic radiative and radiationless yields for K and L shells. *J. Phys. Chem. Ref. Data* **8** 307-327

[7] Krause M O and Oliver J H 1979 Natural widths of atomic K and L levels, Kα X-ray lines and several KLL Auger lines. *J. Phys. Chem. Ref. Data* **8** 329-338

[8] Harada T and Kita T 1980 Mechanically ruled aberration-corrected concave gratings. *Appl. Optics* **19** 3987-3993

[9] Koike M, Yamazaki T and Harada Y 1999 Design of holographic gratings recorded with aspheric wave-front recording optics for soft X-ray flat-field spectrographs. *J. Electron Spectrosc. Rel. Phenom.* **101-103** 913-918

[10] Terauchi M, Takahashi H, Handa N, Murano T, Koike M, Kawachi T, Imazono T, Koeda M, Nagano T, Sasai H, Oue Y, Yonezawa Z and Kuramoto S 2012 Ultrasoft-X-ray emission spectroscopy by using a newly designed WDS spectrometer attached to a transmission electron microscope. *J. Electron Microsc.* **61** 1-8

[11] Terauchi M, Takahashi H, Handa N, Murano T, Koike M, Kawachi T, Hasegawa N, Imazono T, Koeda M, Nagano T, Sasai H, Oue Y, Yonezawa Z and Kuramoto S 2012 A new grating X-ray spectrometer for 2 - 4 keV enabling a separate observation of In-Lβ and Sn-Lα emissions of indium-tin-oxide. *Microscopy* **62** 391-395

[12] Terauchi M, Takahashi H, Takakura M, Murano T, Koike M, Imazono T, Nagano T, Sasai H and Koeda M 2016 Chemical state analysis of trace-boron by using an improved SEM-SXES. *Microsc. Microanal.* **22** (Suppl. 3) 414-415

[13] Takeda M, Terui M, Takahashi N and Ueda N 2006 Improvement of thermoelectric properties of alkaline-earth hexaborides. *J. Solid State Chem.* **179** 2823-2826

[14] Kuribayashi H, Makino S, and Takeda M 2014 Synthesis and characterization of p-type CaB_6. *Abstract of ISBB18*. (Honolulu, 31 August -5 September) 148

[15] Terauchi M 2019 Information of valence charge of 3d transition metal elements observed in L-emission spectra. *Microscopy*, accepted

[16] Terauchi M, Koshiya S and Kimoto K 2017 Information observed in Ti-Lα,β and Ti-Ll,η emission lines of Ti and its oxides. *IOP Conf. Series: Mater. Sci. Engng.* **304** 012018-1-6

[17] Grebennikov V I, Galakhov V R, Finkelshtein L D, Ovechkina N A and Kurmaev E Z 2003 Effect of atomic magnetic moments on the relative intensity of the Lβ and Lα components in X-ray emission spectra of 3d transition metal oxides. *Phys. Solid State* **45** 1048-1055

[18] Hatano T, Koike M, Nishihara H, Pirozhkov A S, Terauchi M, Sasai H and Nagano T 2018 Enhancement of diffraction efficiency and spectral flux of laminar-type diffraction gratings coated with Ni/La/C layers in soft X-ray region. *Abstract of SRI2018*. (Taipei, 10-15 June) 232

[19] Terauchi M, Koike M, Fukushima K and Kimura A 2010 Development of wavelength-dispersive soft X-ray emission spectrometer for transmission electron microscopes – an introduction of valence electron spectroscopy for transmission electron microscopy. *J. Electron Microsc.* **59** 251-261